

## Shear beams with indirect supports – numerical modeling and experimental assessment

M. Pimentel<sup>1</sup>, Paulo Cachim<sup>2</sup>, J. Figueiras<sup>1</sup>

### Summary

This article presents current research developed at Labest (FEUP structural concrete laboratory) in order to investigate the behavior of deep beams with indirect supports. Intending to analyze the behavior of a water treatment plant with large rectangular reservoirs, three reduced scale deep beams specimens were built to evaluate the numerical model performance in capturing a possible shear failure mechanism. Numerical analysis of real size similar beams has shown that size effects associated with this kind of failure can be modeled. Some numerical parameters of the constitutive model are discussed concerning their relevance to the physical phenomena under analysis.

### Introduction

Deep beams are a common structural element in civil engineering where shear forces play a major role in the safety assessment. Increased complexity is recognized involving the dimensioning process when shear failures are expected, especially if indirect supports are used and/or suspended loads are present. The classical design procedure is based on strut and tie models following the principal elastic stresses path. This is an equilibrium method wherein the compatibility conditions are not fulfilled. Two different failure mechanisms are presented in figures 1 and 2.

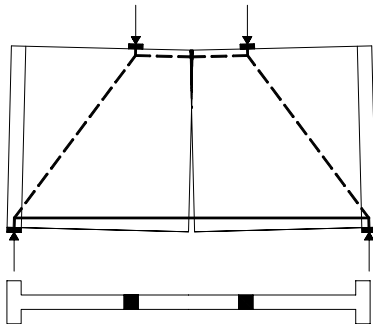


Figure 1 – Flexural failure mechanism

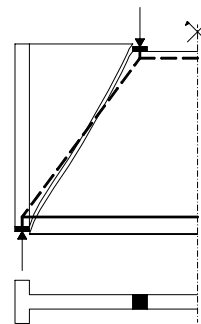


Figure 2 – Shear failure mechanism

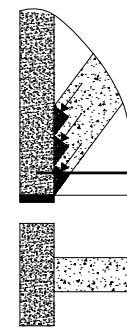


Figure 3 – Indirect support effect.

On the flexural type mechanism the equilibrium scheme proposed by the strut and tie model seems quite evident. On the shear/compression type mechanism, of fragile

<sup>1</sup> Faculty of Engineering of the University of Porto (FEUP), Porto, Portugal

<sup>2</sup> University of Aveiro, Aveiro, Portugal.

nature, a shear crack band crosses the load path. This crossing is only possible if the crack opening is limited in order to keep the interlock between crack surfaces. In other words, the structure may not have the necessary ductility to ensure the idealized equilibrium scheme. In case of indirect supports (figure 3) the stresses flow between two boundaries with different stiffness being transmitted by a shear/compression mechanism, which may increase the beam fragile type of shear failure.

### Experimental setup

Laboratorial model geometry and the adopted reinforcement are presented in figures 4 and 5. Only one of the tested specimens is going to be presented, more information about the experimental setup can be found in reference [1]. In this specimen main tie rebars are distributed over a 4 cm height that can be considered 2.75 cm away from the bottom for equilibrium purposes. A reinforcement grid of very mild steel was placed over the beam height so that the minimum reinforcement requirement is not fully accomplished. The beam was designed in such a way that shear and flexural failures can be reached at very close levels.

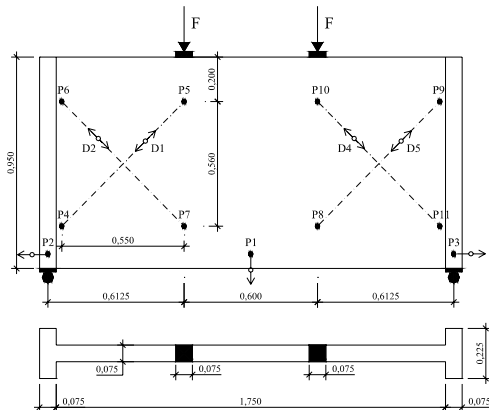


Figure 4 – Geometry and location of the displacement measures.

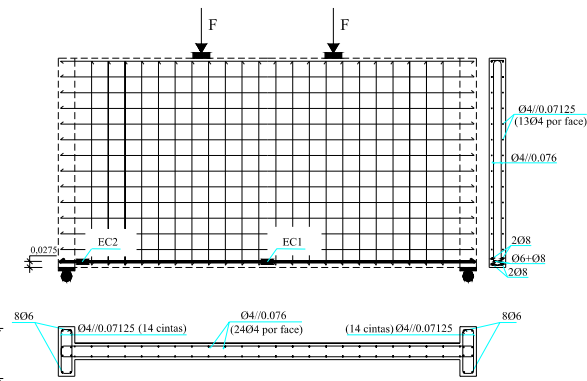


Figure 5 – Reinforcement and strain-gauges location.

The model was instrumented with six Lvdts and two strain-gauges glued on to the rebars. The load was applied under load control up to 150 kN per each hydraulic actuator. For the reload process displacement control was activated and the experiment proceeded until the capacity of the hydraulic pressure system was reached. At this stage the failure mechanism was not reached but a probable shear/compression failure is about to occur as can be observed from the crack pattern (Fig.10). The measurements show that the reinforcement is in yielding process and that no substantial load increase can be carried out. A new setup is being made in order to confirm this beam failure mechanism.

### Numerical model

A smeared crack model with strain decomposition currently implemented in Diana 8.1 finite element package was used (details can be found in references [1-6]). The formulation allows for multiple cracks in each integration point and crack initiation criteria is governed by the simultaneous satisfaction of the tension cut-off condition and the violation of the threshold angle between cracks ( $\alpha$ ). For the elements near main tie rebars a tension stiffening concept following the diagram presented in figure 6 was introduced. In regions where reinforcement is not able to control crack propagation a linear tension softening diagram based on concrete fracture energy ( $G_f$ ) was used with ultimate crack strain given by

$$\varepsilon_u^{cr} = \frac{2G_f}{f_t h} \quad (1)$$

In expression (1)  $h$  is the crack band width, considered equal to the square root of the eight node (2x2 Gaussian integration) finite element area, and  $f_t$  the concrete tension strength. This approximation for the crack band width  $h$  may not be acceptable for distorted elements. Crack shear behavior is modeled through a constant shear retention concept with shear stiffness being reduced from  $G$  to  $\beta G$  after crack opening.

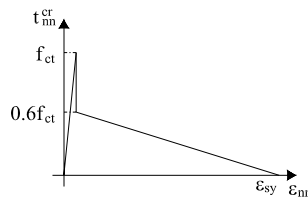


Figure 6 – Tension stiffening diagram.

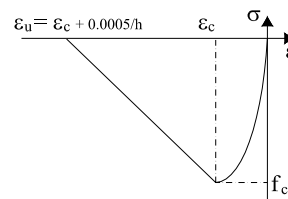


Figure 7 – Uniaxial compression curve.

Under compressive stress states concrete is treated along the lines of plasticity theory. For plane stress states a Drucker-Prager failure surface with a 10 degrees friction angle fits the biaxial results of Kupfer and Gerstle [5]. An associated flow rule with hardening coesion was used, with the hardening diagram fitting the CEB uniaxial compression curve (figure 7). The softening branch was determined by considering that compressive failure is localized in a plane normal to the direction of compressive principal stress. It was assumed that all compressive displacements and energy dissipation are localized in this plane and that this displacement does not depend on the structure size. From these assumptions compressive fracture energy is indirectly defined. Based on experimental evidence for regular concrete the value of 0.5 mm was used for this localized displacement [7].

Reinforcement is modeled either with truss elements or with zero shear stiffness orthotropic plane elements. Perfect bond is assumed so that reinforcement nodal displacements are interpolated from concrete element nodes.

### Numerical vs. experimental results

Concrete properties used are given by: compressive strength  $f_c = 45$  MPa, tensile strength  $f_t = 3.2$  MPa, shear retention factor  $\beta = 0.10$ , fracture energy  $G_f = 100$  N/mm<sup>2</sup>, Poisson's ratio  $\nu = 0.15$ . Reinforcement steel yielding strength was  $f_y = 530$  MPa, except for the 4 mm rebars that had  $f_y = 180$  MPa.

In general very good approximation to all experimental results was obtained as can be seen in the examples of figures 8 and 9. All the numerical results were obtained prior to the experiments so no attempt has been made to fit the experimental curves. Better curve fitting, including closer crack patterns, can be obtained using higher fracture energy. This can reflect the effect of the small amount of reinforcement placed over the beam height, since small aggregates were used. Using a higher shear retention factor (say  $\beta = 0.25$ ) the response is approximately the same resulting in slight increasing in the ultimate displacements. Modifying the concrete strength different ultimate loads are obtained.

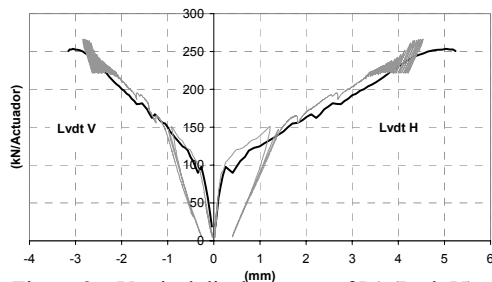


Figure 8 – Vertical displacement of P1 (Lvdt V) and relative displacements between P2 and P3 (Lvdt H).

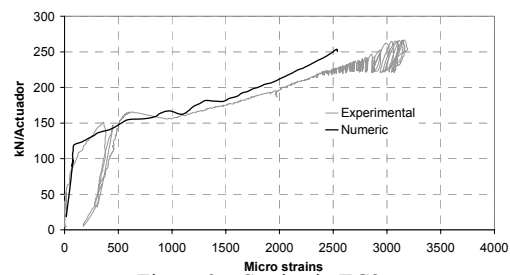


Figure 9 – Strains in EC2.

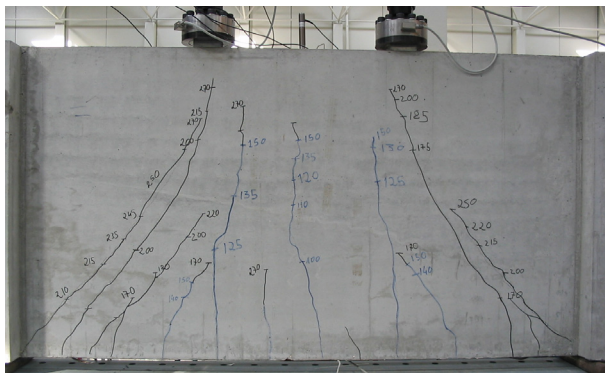


Figure 10 – Experimental crack pattern.

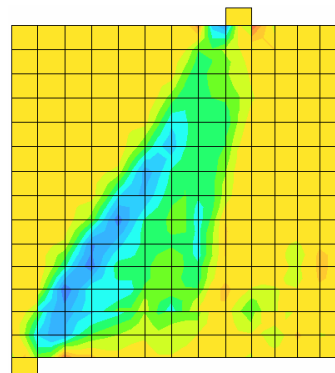


Figure 11 – Mesh with  $\gamma_{xy}$  contour levels.

Numerical failure occurs after main reinforcement yielding with fracture zone localization along a diagonal shear crack (Fig.11). All Gauss points along the fracture region are cracked except for one placed on the left side of the load platen. Divergence of the numerical procedure occurs after 3 converged increments with this integration point in the softening regime, with corresponding decrease of the applied load. Therefore it can be justified that this divergence corresponds to a physical shear/compression failure. As stated in [2] it is incorrect to simply identify structural failure with divergence of the iterative process since it might be caused by an insufficiency of the numerical procedure and have therefore no physical meaning. The numerical failure mechanism is very similar to other shear/compression mechanisms observed experimentally with concrete crushing on diagonal crack tip.

### Size effect

To perform numerical analysis on real scale structures it is mandatory to assess the capability of the numerical model in the evaluation of size effects commonly associated with shear failures. A real size deep beam was analysed. Dimensions of this beam are scaled up to a factor of  $s_f = 8.41$  from laboratorial model dimensions and are similar to the real structure that is under design considerations. For dimensionless parameter allowing size effect evaluation the average shear stress given by expression (2) was chosen, where  $F$  is the force in each loading platen,  $h$  and  $b$  are beam height and thickness, respectively.

$$\tau_{med} = \frac{F}{bh} \quad (2)$$

To maintain the same average shear stress at failure the ultimate load on the real scale structure and amount of reinforcement are obtained multiplying the laboratorial model quantities by  $s_f^2 = 8.41^2$ . Reinforcement was placed at the same relative positions as it is in the reduced model.

Numerical analysis gave a failure mechanism with exactly the same characteristics as the previous one but with ultimate average shear stress 20% lower than in the reduced model. Failure occurred prior to the yielding of main reinforcement. This size effect could be even more pronounced if both failures occurred with reinforcement within the elastic range. In figure 13 a graph is given where the average shear and horizontal strains over the shear span are plotted against the average shear stress.

### Conclusions

The used numerical model was found to provide accurate calculations of strength, load-deformation response and failure mode of laboratorial deep beams with indirect supports. It was possible to identify and justify numerical shear/compression failures. The influence on the results of some model parameters was discussed. Size effect was

detected in the numerical simulations. Experimental and numerical evidence seem to show that the use of a more distributed arrangement of reinforcement along the bottom tie cannot delay the shear failure. In proceeding work this subject as well as the effect of prestress will be discussed.

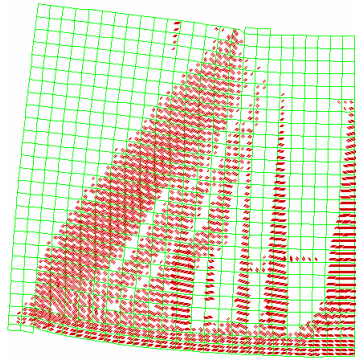


Figure 12 – Deformed mesh vectors normal to crack surfaces.

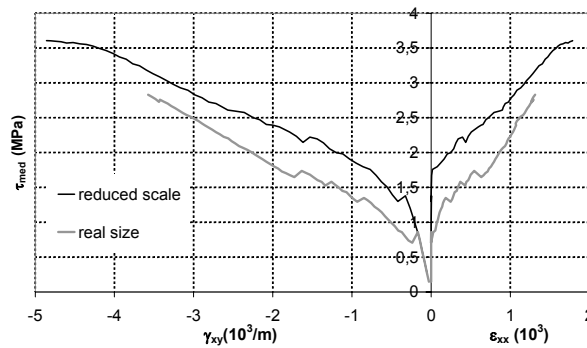


Figure 13 – Comparative results between real scale and reduced scale beams.

### References

1. Pimentel, M., et al. *Modelação numérica e validação experimental do comportamento de vigas-parede com apoios indirectos*. in *Congresso de Métodos Computacionais em Engenharia*. 2004. Lisboa.
2. Borst, R. and P. Nauta, *Non-orthogonal cracks in a smeared finite element model*. *Engineering Computations*, 1985. **2**: p. 35-46.
3. Borst, R., *Smeared cracking, plasticity, creep and thermal loading - A unified approach*. *Computer Methods in Applied Mechanics and Engineering*, 1987. **62**(1): p. 89-110.
4. Rots, J.G. and J. Blaauwendraad, *Crack models for concrete: Discrete or smeared? Fixed, multi-directional or rotating*. *Heron*, 1989. **34**(1).
5. Vários, *User's Manual release 8.1*. DIANA - Finite Element Analysis, ed. F.C. Witte and W.P. Kikstra. Vol. Material Library. 2002, Delft: TNO Building and Construction Research.
6. Barros, J., *Comportamento do Betão Reforçado com Fibras - Análise Experimental e Modelação Numérica*. 1995, Faculdade de Engenharia da Universidade do Porto: Porto.
7. Cervenka, V., L. Jendele, and J. Cervenka, *ATENA Program Documentation Part 1 - Theory*. 2002, Cervenka Consulting: Prague.